Visible and near-infrared emitting heterotrimetallic lanthanide–aluminum–sodium 12-metallacrown-4 compounds: discrete monomers and dimers

Svetlana Eliseeva, Jordan Travis, Sarah Nagy, Alyssa Smihosky, Collin Foley, Abigail Kauffman, Curtis Zaleski, Stéphane Petoud

ARTICLE

Visible and Near-infrared Emitting Heterotrimetallic Lanthanide-Aluminum-Sodium 12-Metallacrown-4 Compounds: Discrete Monomers and Dimers

Received 00th January 20xx,
Accepted 00th January 20xx

DOI: 10.1039/x0xx00000x

Svetlana V. Elisseva,[a*] Jordan R. Travis,[b] Sarah G. Nagy,[b] Alyssa M. Smihosky,[b] Collin M. Foley,[b] Abigail C. Kauffman,[b] Curtis M. Zaleski,[b*] and Stéphane Petoud[a*]

The luminescent properties of two types of heterotrimetallic aluminum-lanthanide-sodium 12-metallacrown-4 compounds are presented here, LnNa(ben)$_4$[12-MC$_{Al(III)N(shi)}$-4] (**LnAl$_4$Na**) and {LnNa[12-MC$_{Al(III)N(shi)}$-4]}$_2$(iph)$_4$ (**Ln$_2$Al$_8$Na$_2$**), where Ln = Gd^{III}, Tb^{III}, Er^{III}, and Yb^{III}, MC is metallacrown, ben$^-$ is benzoate, shi^{3-} is salicylhydroximate, and iph^{2-} is isophthalate. The aluminum-lanthanide-sodium metallacrowns formed with benzoate are discrete molecules while, upon replacement of the benzoate by the dicarboxylate isophthalate, two individual metallacrowns can be joined to form a dimer. In the solid state, the terbium complex of each structure type displays emission in the visible region, and the erbium and ytterbium complexes emit in the near-infrared. The luminescence lifetimes (τ_{obs}) and quantum yields have been collected under ligand excitation (Q^L_{Ln}) for both **LnAl$_4$Na** monomers and **Ln$_2$Al$_8$Na$_2$** dimers. Several of these values tend to be shorter (luminescence lifetimes) and smaller (quantum yields) than the corresponding values recorded for the structurally similar gallium-lanthanide monomer and dimer 12-MC-4 molecules. However, the quantum yield value recorded for the visible emitting **Tb$_2$Al$_8$Na$_2$** dimer, 43.9%, is the highest value observed in the solid state to date for a Tb^{III} based metallacrown.

Introduction

Metallacrowns (MCs), the functional and structural inorganic analogues to crown ethers, provide a pathway to self-assemble heterometallic macrocyclic molecules in a controllable and predictable manner.[1] Archetypal metallacrowns contain a metal-nitrogen-oxygen repeat unit in a cyclic fashion akin to the carbon-carbon-oxygen repeat unit of a crown ether. In addition, like crown ethers, metallacrowns contain a central cavity that can bind a metal ion via several oxygen atoms. While the same type of metal ion can be used for both the ring and the central cavity positions, it is commonplace for the ring metal ions and central cavity metal ion to be different. The choice of metal ions in these positions can dictate the properties of the metallacrown; thus, the molecules can be tailored to address the needs of a specific application. For example, the use of lanthanide ions in combination with transition metal ions can lead to the formation of 3*d*-4*f* heterometallic MCs with single-molecule magnet properties.[2,3] In addition, the self-assembly process driving the formation of MCs allows the molecules to be functionalized while retaining structural similarities between related molecules. In a series of manganese-lanthanide 12-MC-4 complexes LnNaX$_4$[12-MC$_{Mn(III)N(shi)}$-4], where X is a carboxylate anion and shi^{3-} is salicylhydroximate, the structure of the MC can easily be conserved as the identity of the carboxylate is varied.[3,4] A large variety of carboxylate anions have been used including acetate, benzoate, trimethylacetate, hydroxybenzoates (2, 3, and 4 positions), and halogenated benzoates (chloro, bromo, and iodo in the 2, 3, or 4 positions).[3,4] Independent of the identity of the carboxylate anion, the MC has an overall square shape with a Mn-N-O repeat unit about the MC ring and lanthanide and sodium ions are captured on opposite sides of the central cavity. Thus, the properties of these molecules can be finely tuned by the judicious choice of the nature of the carboxylate anions. Indeed, when the magnetic properties of the DyNaX$_4$[12-MC$_{Mn(III)N(shi)}$-4] complexes synthesized with acetate, benzoate, trimethylacetate, and salicylate were investigated, only the salicylate version behaved as a single-molecule magnet.[3]

Not only can the ligands of the metallacrowns be varied with structural integrity being maintained, but the ring metal ions can also be varied while retaining a structural similarity. If the ring manganese(III) ions of the LnNaX$_4$[12-MC$_{Mn(III)N(shi)}$-4] structures are replaced with gallium(III), the analogous MCs can be produced.[5] One advantage of the gallium metal ion in MCs is that the luminescent properties of the central lanthanide ions can be exploited. It is well established that lanthanide ions can be highly luminescent with long-lived excited electronic states, have large energy differences between excitation and emission wavelengths (pseudo-Stoke shifts), and can emit in the UV, visible, and NIR regions.[6] For example, lanthanide clusters are known to be particularly luminescent materials with potential applications such as biological imaging and sensing.[7] Gallium(III) with its closed-shell electronic structure does not quench the excited states of lanthanide ions in MCs as would the manganese(III) ions of the [12-MC$_{shi}$-4] molecules. Indeed, we have recently reported the luminescent properties of gallium-lanthanide [12-MC$_{shi}$-4] molecules.[5,8-12] A series of (Hpy)Ln(benzoate)$_4$[12-MC$_{Ga(III)N(shi)}$-4]

[a] *Centre de Biophysique Moléculaire, CNRS UPR 4301, 45071 Orléans Cedex 2, France.*
[b] *Department of Chemistry and Biochemistry, Shippensburg University, 1871 Old Main Dr., Shippensburg, PA 17257.*
*corresponding email: svetlana.eliseeva@cnrs-orleans.fr, cmzaleski@ship.edu, and stephane.petoud@inserm.fr.
Electronic Supplementary Information (ESI) available: Images of all investigated metallacrowns under ambient conditions and excitation at 254 nm. See DOI: 10.1039/x0xx00000x

compounds, where Hpy^+ is pyridinium, are highly luminescent in both the visible and NIR.[5] In addition, the Sm^{III} version can act as a sensor for G-quadruplex DNA[8], and the Dy^{III} analogue can emit white light.[9] These molecules are structurally similar to the DyNa(benzoate)$_4$[12-MC$_{Mn(III)N(shi)}$-4] discussed above except with the use of the uncoordinated countercation pyridinium instead of a coordinated sodium ion. If the benzoate anions are replaced with the dicarboxylate isophthalate, two Ln[12-MC$_{shi}$-4] units can be linked together to form a dimer, {Ln[12-MC$_{Ga(III)N(shi)}$-4]}$_2$(iph)$_4$.[10] These molecules are also highly luminescent and can meet the requirements of applications such as luminescent molecular nanothermometers.[10,11] In addition, if iodinated versions of isophthalate or salicylhydroximate are incorporated into the dimer, the molecules can be used as X-ray computed tomography (XCT) imaging agents.[12] Some of the dimers contain uncoordinated ammonium countercations while others have coordinated sodium ions. The sodium ions may bind to the central cavity of the 12-MC-4 moiety as in the monomer LnNaX$_4$[12-MC$_{Mn(III)N(shi)}$-4] molecules but, in some instances, the sodium ions bind to the side of the dimer structures. The dimer motif can also accommodate Mn^{III} ions in ring positions as we and others have also reported analogous structures with sodium as the counteraction.[2m,13] For the {LnNa[12-MC$_{Mn(III)N(shi)}$-4]}$_2$(iph)$_4$ dimers, the sodium cation has only been reported binding to the central cavity of the 12-MC-4 moiety.

Expanding on the gallium-lanthanide work, we decided to investigate aluminum-based metallacrowns. Aluminum has not generally been incorporated into the ring structure of metallacrowns as the research has mainly focused on *d*-block metals as opposed to *p*-block metals. Besides gallium, tin[14] and tellurium[15] are the only *p*-block metals that have been included in the archetype MC ring structure (N-O repeat unit). We questioned if the smaller ionic radius of Al^{III} (calculated according to Shannon[16] as 0.535 Å for CN = 6) versus Mn^{III} (0.645 Å; CN = 6 and high spin) and Ga^{III} (0.620 Å; CN = 6) would induce the shrinking of the size of the MC cavity and prohibit the binding of the Ln^{III} ion. However, the synthesis of aluminum-lanthanide-sodium metallacrowns proved to be facile chemistry, and we recently reported the structures of the analogous monomer LnNa(ben)$_4$[12-MC$_{Al(III)N(shi)}$-4] molecules and dimer {LnNa[12-MC$_{Al(III)N(shi)}$-4]}$_2$(iph)$_4$ molecules, both with coordinated sodium ions.[17] A structural comparison of the aluminum and manganese Ln[12-MC$_{shi}$-4] molecules reveals that there are minimal changes to the [12-MC$_{shi}$-4] central cavity distances and that the nature of the ring metal ion does not significantly alter the MC framework.[17] Thus, these aluminum-based metallacrowns are structurally similar to the manganese and gallium versions discussed above. Herein we report the luminescent properties of the two types Ln[12-MC$_{Al(III)N(shi)}$-4] compounds: LnNa(ben)$_4$[12-MC$_{Al(III)N(shi)}$-4] (**LnAl$_4$Na**) and {LnNa[12-MC$_{Al(III)N(shi)}$-4]}$_2$(iph)$_4$ (**Ln$_2$Al$_8$Na$_2$**), where Ln = Gd^{III}, Tb^{III}, Er^{III}, and Yb^{III}.

Experimental

Synthesis of Compounds

The LnNa(ben)$_4$[12-MC$_{Al(III)N(shi)}$-4] and {LnNa[12-MC$_{Al(III)N(shi)}$-4]}$_2$(iph)$_4$ compounds were prepared as previously reported.[17]

GdNa(ben)$_4$[12-MC$_{Al(III)N(shi)}$-4](H$_2$O)$_4$•3DMF•1.5H$_2$O, **GdAl$_4$Na**. Elemental analysis for $C_{65}H_{68}Al_4GdN_7NaO_{28.5}$ (FW = 1691.43 g/mol): Found (%) H = 3.74, C = 45.79, N = 6.26; Calculated (%) H = 4.05, C = 46.16, N = 5.80.

TbNa(ben)$_4$[12-MC$_{Al(III)N(shi)}$-4](H$_2$O)$_4$•6.5DMF, **TbAl$_4$Na**. Elemental analysis for $C_{75.5}H_{89.5}Al_4N_{10.5}NaO_{30.5}Tb$ (FW = 1921.91 g/mol): Found (%) H = 4.76, C = 47.03, N = 7.55; Calculated (%) H = 4.69, C = 47.18, N = 7.65.

ErNa(ben)$_4$[12-MC$_{Al(III)N(shi)}$-4](H$_2$O)$_4$•4DMF•1.5H$_2$O, **ErAl$_4$Na**. Elemental analysis for $C_{68}H_{75}Al_4ErN_8NaO_{29.5}$ (FW = 1774.54 g/mol): Found (%) H = 4.00, C = 45.74, N = 6.70; Calculated (%) H = 4.26, C = 46.02, N = 6.31.

YbNa(ben)$_4$[12-MC$_{Al(III)N(shi)}$-4](H$_2$O)$_4$•4.5DMF, **YbAl$_4$Na**. Elemental analysis for $C_{69.5}H_{75.5}Al_4N_{8.5}NaO_{28.5}Yb$ (FW = 1789.84 g/mol): Found (%) H = 4.40, C = 46.54, N = 6.75; Calculated (%) H = 4.25, C = 46.64, N = 6.65.

{GdNa[12-MC$_{Al(III)N(shi)}$-4]}$_2$(iph)$_4$(DMF)$_2$(H$_2$O)$_8$•6.5DMF•H$_2$O, **Gd$_2$Al$_8$Na$_2$**. Elemental analysis for $C_{113.5}H_{125.5}Al_8Gd_2N_{16.5}Na_2O_{57.5}$ (FW = 3217.12 g/mol): Found (%) H = 3.57, C = 42.33, N = 7.49; Calculated (%) H = 3.93, C = 42.37, N = 7.18.

{TbNa[12-MC$_{Al(III)N(shi)}$-4]}$_2$(iph)$_4$(DMF)$_2$(H$_2$O)$_8$•5DMF•2H$_2$O, **Tb$_2$Al$_8$Na$_2$**. Elemental analysis for $C_{109}H_{117}Al_8N_{15}Na_2O_{57}Tb_2$ (FW = 3128.84 g/mol): Found (%) H = 3.40, C = 41.52, N = 7.11; Calculated (%) H = 3.77, C = 41.84, N = 6.71.

{ErNa[12-MC$_{Al(III)N(shi)}$-4]}$_2$(iph)$_4$(DMF)$_4$(H$_2$O)$_{10}$•2.5DMF, **Er$_2$Al$_8$Na$_2$**. Elemental analysis for $C_{107.5}H_{113.5}Al_8Er_2N_{14.5}Na_2O_{56.5}$ (FW = 3108.97 g/mol): Found (%) H = 3.31, C = 41.14, N = 6.91; Calculated (%) H = 3.68, C = 41.53, N = 6.53.

{YbNa[12-MC$_{Al(III)N(shi)}$-4]}$_2$(iph)$_4$(DMF)$_2$(H$_2$O)$_8$•6DMF•4.5H$_2$O, $Yb_2Al_8Na_2$. Elemental analysis for $C_{112}H_{129}Al_8N_{16}Na_2O_{60.5}Yb_2$ (FW = 3275.21 g/mol): Found (%) H = 3.52, C = 40.67, N = 7.28; Calculated (%) H = 3.96, C = 41.07, N = 6.84.

Elemental Analyses

Analyses for **TbAl$_4$Na** and **YbAl$_4$Na** were performed by Atlantic Microlabs Inc (Norcross, Geogia, USA)**,** and analyses for **GdAl$_4$Na**, **ErAl$_4$Na**, **Gd$_2$Al$_8$Na$_2$**, **Tb$_2$Al$_8$Na$_2$**, **Er$_2$Al$_8$Na$_2$**, and **Yb$_2$Al$_8$Na$_2$** were performed at the Université de Rennes (Rennes, France).

Luminescence Measurements

Luminescence data were collected on solid state samples placed in 2.4 mm i.d. quartz capillaries (Fig. S1). Steady-state emission and excitation spectra were measured on a custom-designed Horiba Scientific Fluorolog 3 spectrofluorimeter equipped with either a visible photomultiplier tube (PMT) (220–850 nm, R928P; Hamamatsu) or a NIR PMT (950–1650 nm, H10330-75; Hamamatsu) upon excitation with a continuous Xenon lamp. All excitation and emission spectra were corrected for the instrumental functions. Luminescence lifetimes (τ_{obs}) were determined under excitation at 355 nm provided by a Nd:YAG laser (YG 980; Quantel). Signals were detected in the visible or NIR ranges using an iHR320 monochromator (Horiba Scientific) equipped with a Hamamatsu

R928P and H10330-75 PMTs. The output signal from the detector was fed into a 500 MHz bandpass digital oscilloscope (TDS 754C; Tektronix), transferred to a PC for data processing with the program Origin 8®. Luminescence lifetimes are averages of at least three independent measurements. Ln^{III}-centered quantum yields under ligands excitation (Q_{Ln}^{L}) at 330 nm were determined with the Fluorolog 3 spectrofluorimeter based on an absolute method with the use of an integration sphere (Model G8, GMP SA, Renens, Switzerland). Each sample was measured several times under comparable experimental conditions, varying the position of samples. Estimated experimental error for quantum yield determination is ~10 %. Phosphorescence spectra of **$GdAl_4Na$** and **$Gd_2Al_8Na_2$** in the solid state at 77 K were acquired on a Horiba-Jobin-Yvon Fluorolog 3 spectrofluorimeter in a time-resolved mode. Based on the Gaussian decomposition of the phosphorescence spectra the energies of the 0–0, 0–1, and 0–2 vibrational transitions were determined.

Results and discussion

Structural Description of the Metallacrowns

The single crystal X-ray structures of the $LnNa(ben)_4[12\text{-}MC_{Al(III)N(shi)}\text{-}4]$ (**$LnAl_4Na$**) and $\{LnNa[12\text{-}MC_{Al(III)N(shi)}\text{-}4]\}_2(iph)_4$ (**$Ln_2Al_8Na_2$**) compounds (Fig. 1-3), where Ln = Gd^{III}, Tb^{III}, Er^{III}, and Yb^{III}, have been previously reported.[17] Therefore, only an overview of the structures will be provided here. For both the **$LnAl_4Na$** and **$Ln_2Al_8Na_2$** molecules, their respective structures are built upon a $[12\text{-}MC_{Al(III)N(shi)}\text{-}4]$ framework where four ring Al^{III} ions and four N-O repeat units generate the metallacrown connectivity. The ligand salicylhydroximate (shi^{3-}) provides the N-O linkages and places the Al^{III} ions at an angle of 90° relative to each other via five- and six-membered fused chelate rings. This organization generates an overall square metallacrown framework that is slightly domed away from the central Ln^{III} ion. In both the **$LnAl_4Na$** and **$Ln_2Al_8Na_2$** compounds, a Ln^{III} ion is coordinated in the central MC cavity by the oxime oxygen atoms. In the **$LnAl_4Na$** compounds, the Ln^{III} ion is further tethered to the MC framework by four benzoate (ben^{-}) anions that bridge via the carboxylate groups between the Ln^{III} ion and the four ring Al^{III} ions. If the benzoate anion is replaced by the dicarboxylate anion isophthalate (iph^{2-}), then two $Ln[12\text{-}MC_{Al(III)N(shi)}\text{-}4]$ units can be connected together to form a dimer of MCs: **$Ln_2Al_8Na_2$**. The binding of the isophthalate is analogous to that of the benzoate as the dicarboxylate bridges between the central Ln^{III} ion and the four Al^{III} ions on each end of the dimer. For the **$LnAl_4Na$** compounds, a sodium ion is also captured in the central cavity opposite of the Ln^{III} ion. The coordination sphere of the sodium ion is completed by water molecules. For the **$Ln_2Al_8Na_2$** compounds, the sodium ions have two coordination modes. For **$Tb_2Al_8Na_2$** and **$Yb_2Al_8Na_2$**, the sodium ions bind to the central cavity opposite of the Ln^{III} ions as observed in the **$LnAl_4Na$** compounds. However, for **$Er_2Al_8Na_2$**, the sodium ions bind on the side of the dimer by coordinating to phenolate and carboxylate oxygen atoms belonging to two different shi^{3-} ligands and the carboxylate oxygen atom of an iph^{2-} ligand. In either of these binding positions, the coordination sphere of the sodium ions is completed by solvent molecules: water and/or DMF molecules. At this time, we have not rationalized the factors that govern the location where the sodium ions bind to the dimer MCs.

The Ln^{III} ions in both **$LnAl_4Na$** and **$Ln_2Al_8Na_2$** are eight-coordinate upon binding to four oxime oxygen atoms of the MC cavity and four carboxylate oxygen atoms belonging to either benzoate or iph^{2-}. A continuous shape measures (CShM) analysis (*SHAPE 2.1*[18]*)* indicates that the coordination geometry around the lanthanide ion is best described as a square antiprism (D_{4d}).[17] For both sets of compounds, the Al^{III} ions are six-coordinate by binding two *trans* shi^{3-} ligands in the equatorial plane and the axial coordination is completed by a carboxylate oxygen atom of a benzoate or a iph^{2-} ligand and an oxygen atom of either a water or DMF molecule. The CShM analysis indicates an octahedral (O_h) geometry around the aluminum ions.[17] The sodium ions of **$LnAl_4Na$**, **$Tb_2Al_8Na_2$**, and **$Yb_2Al_8Na_2$** are nine-coordinate with a distorted spherical capped square antiprism geometry (C_{4v}).[17] The coordination sphere is composed of four oxime oxygen atoms from the MC cavity, four water molecules, and one carbonyl oxygen atom from a disordered DMF molecule. For **$Er_2Al_8Na_2$**, the sodium ions are six-coordinate, and the CShM analysis reveals that the geometry is best described as a severely distorted octahedron.[17]

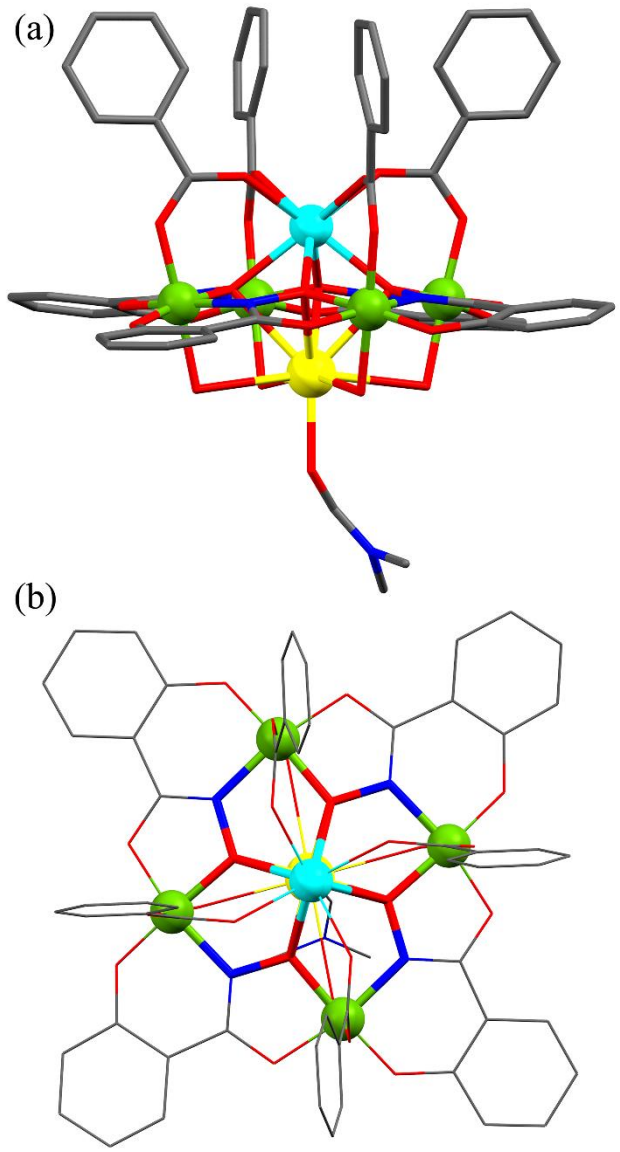

Fig. 1. X-ray crystal structure of **YbAl$_4$Na** with the metal ions displayed as spheres. (a) side view and (b) view along the pseudo-C_4 axis through the Yb^{III} and Na$^+$ ions with the metallacrown N-O connectivity between the Al^{III} ions being highlighted. Hydrogen atoms, lattice DMF and water molecules, and disorder have been omitted for clarity. Color scheme: light blue - ytterbium; green - aluminum; yellow - sodium; red - oxygen; dark blue - nitrogen; and gray - carbon.

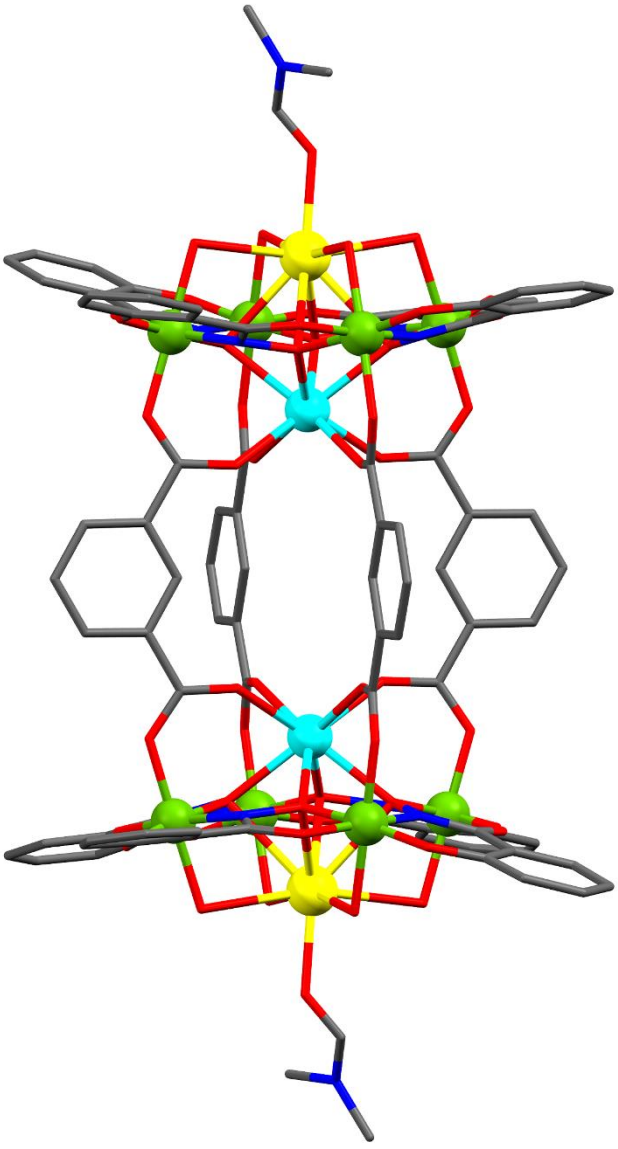

Fig. 2. Side view of the X-ray crystal structure of **Yb$_2$Al$_8$Na$_2$** with the metal ions displayed as spheres. The sodium ions (yellow) bind to the 12-MC-4 moieties opposite of the Yb^{III} ions (light blue). See Fig. 1 for additional display details.

Ln^{III}-centered photophysical properties

Upon excitation into ligand-centered levels at 330 nm, **TbAl$_4$Na** and **Tb$_2$Al$_8$Na$_2$** exhibit the characteristic green emission signals of terbium due to $^5D_4 \rightarrow {}^7F_J$ (J = 6–0) transitions (Figs. 4 and S2), while the corresponding ytterbium (**YbAl$_4$Na** and **Yb$_2$Al$_8$Na$_2$**) and erbium (**ErAl$_4$Na** and **Er$_2$Al$_8$Na$_2$**) MCs show bands in the near-infrared (NIR) range arising from the $^2F_{5/2} \rightarrow {}^2F_{7/2}$ (940–1070 nm; Fig. 5) and from the $^4I_{13/2} \rightarrow {}^4I_{15/2}$ (1460–1620 nm; Fig. 6) transitions, respectively. Emission spectra of terbium in **TbAl$_4$Na** and **Tb$_2$Al$_8$Na$_2$** are dominated by the $^5D_4 \rightarrow {}^7F_5$ transition centered at 545 nm. Relative integral intensities of $^5D_4 \rightarrow {}^7F_J/{}^5D_4 \rightarrow {}^7F_5$ transitions (Table 1) are very similar for the monomer MC and the dimer MC. For the investigated monomer and dimer MCs, the Ln^{III} crystal-field splitting of the *f-f* transitions remains the same which is consistent with the similarities of coordination environments and symmetries around

the Ln^{III} ion in both types of studied complexes. Excitation spectra of the MCs upon monitoring the emission at 545 nm for Tb^{III}, 980 nm for Yb^{III}, and 1525 nm for Er^{III} are dominated by broad bands in the UV range up to 360 nm (Fig. 4-6) indicating an efficient sensitization of these Ln^{III} ions through the energy levels of the chromophoric part of the MC scaffold. In addition, in the excitation spectrum of the erbium MCs, sharp bands assigned to *f-f* transitions throughout the visible range are observed, reflecting the possibility of direct excitation of the Er^{III} ion(s). In the case of the terbium MCs, sharp features were detected at 360–380 nm which are, however, of very weak intensity compared to the broad ligand-centered bands.

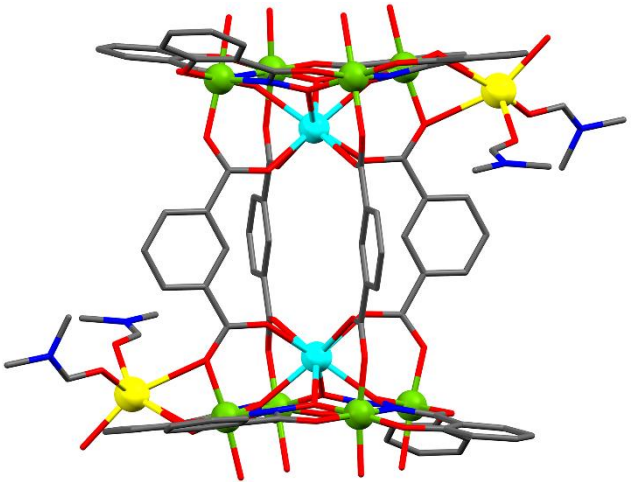

Fig. 3. Side view of the X-ray crystal structure of $Er_2Al_8Na_2$ with the metal ions displayed as spheres. The sodium ions (yellow) bind to the side of the dimer instead of the MC cavity. See Fig. 1 for additional display details.

To quantitatively characterize the luminescence properties of the **LnAl$_4$Na** and **Ln$_2$Al$_8$Na$_2$** MCs, absolute quantum yields were collected under ligands excitation (Q_{Ln}^{L}) on samples in the solid state. Observed luminescence lifetimes (τ_{obs}) were acquired upon ligand excitation, monitoring the signals of the lanthanide cations (Table 2). For the ytterbium and erbium MCs, the values of Q_{Ln}^{L} and τ_{obs} are essentially the same within experimental errors for the monomer molecules and for the dimers. For the terbium MCs, the luminescence lifetimes remain the same for both structure types. Remarkably, the absolute quantum yield Q_{Tb}^{L} increases by a factor 1.8 times from 25(1) % for **TbAl$_4$Na** to 43.9(7) % for **Tb$_2$Al$_8$Na$_2$**. It is important to note that, to date, the quantum yield for the terbrium-aluminum dimer is thus far the highest value recorded for a Tb^{III} MC in the solid state. The quantum yield values measured for the structurally similar monomer **TbGa$_4$** and dimer **Tb$_2$Ga$_8$** metallacrowns are 34.7(1) and 31.2(2)%, respectively.[5,10] In addition, a $[TbGa_8(shi)_8(OH)_4]Na$ double-decker 12-MC-4 molecule, possessing four bridging μ-OH groups between the metallacrown moieties instead of a iph^{2-} group has only a quantum yield of 35(2)% in the solid state.[19]The non-planar metallacrown $Tb(H_2shi)_2(NO_3)[12\text{-}MC_{Ga(III)N(shi)}\text{-}4](pyridine)_4$ has a quantum yield value of only 11.3(5)% in the solid state.[20] Lastly, the [3.3.1] metallacryptate $TbGa_6(H_2shi)(Hshi)(shi)_7(pyridine)$ has a quantum yield of merely 0.189(3)% in the solid state.[21]

Table 1. Integrated intensity ratios ($I_{4\text{-}J}$) of the $^5D_4 \rightarrow {}^7F_J$ transitions normalized with respect to the $^5D_4 \rightarrow {}^7F_5$ transition for **TbAl$_4$Na** and **Tb$_2$Al$_8$** in the solid state for emission spectra collected at room temperature.

Tb^{III} MC	$I_{4\text{-}6}$	$I_{4\text{-}5}$	$I_{4\text{-}4}$	$I_{4\text{-}3}$	$I_{4\text{-}2,1,0}$	I_{tot}
TbAl$_4$Na	0.57	1.00	0.44	0.21	0.09	2.31
Tb$_2$Al$_8$Na$_2$	0.54	1.00	0.51	0.28	0.15	2.48

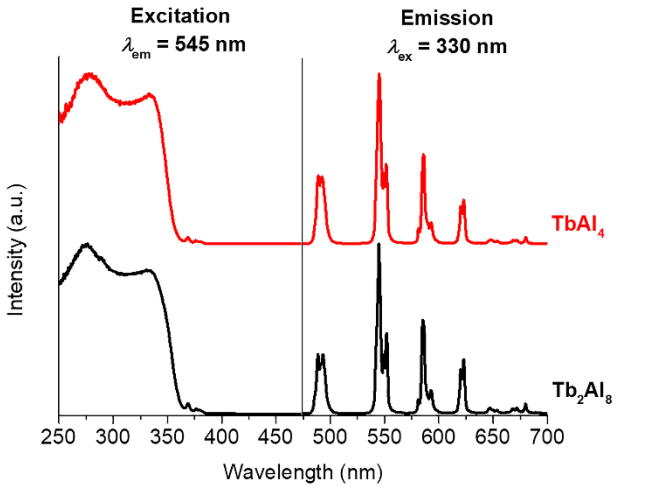

Figure 4. Corrected and normalized excitation and emission spectra of **TbAl$_4$Na** and **Tb$_2$Al$_8$Na$_2$** measured in the solid state at room temperature.

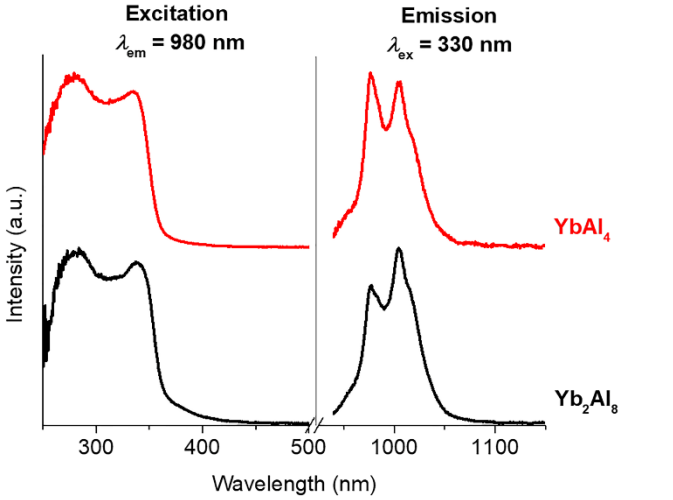

Figure 5. Corrected and normalized excitation and emission spectra of **YbAl$_4$Na** and **Yb$_2$Al$_8$Na$_2$** in the solid state measured at room temperature.

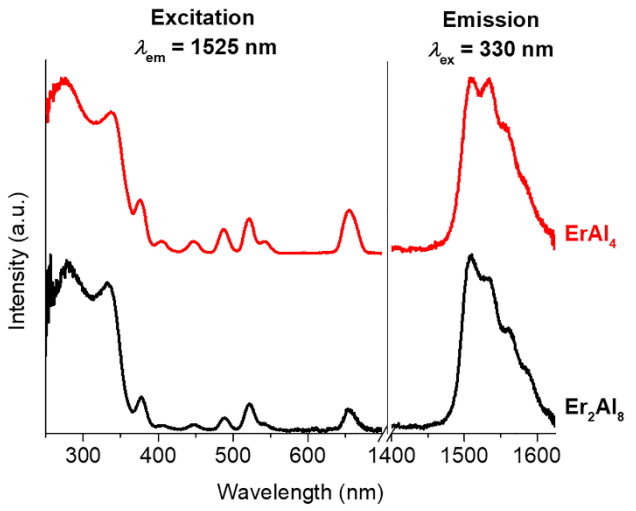

Figure 6. Corrected and normalized excitation and emission spectra of **$ErAl_4Na$** and **$Er_2Al_8Na_2$** in the solid state measured at room temperature.

Table 2. Luminescence lifetimes (τ_{obs}) and Ln^{III}-centered quantum yields obtained under ligand excitation (Q^L_{Ln}) for **LnM_4** and **Ln_2M_8** (M = Al^{III} or Ga^{III}) metallacrowns in the solid state.[a]

MC	τ_{obs} (µs) [b]	Q^L_{Ln} (%) [c]	MC	τ_{obs} (µs) [b]	Q^L_{Ln} (%)[d]
$TbAl_4Na$	1140(10)	25(1)	**$TbGa_4$**[5]	1080(10)	34.7(1)
$Tb_2Al_8Na_2$	1070(10)	43.9(7)	**Tb_2Ga_8**[10]	1410(1)	31.2(2)
$ErAl_4Na$	2.04(1)	0.02(1)	**$ErGa_4$**[5]	6.75(3)	0.044(1)
$Er_2Al_8Na_2$	2.30(2)	0.0198(4)	**Er_2Ga_8**[10]	5.23(2)	0.0057(1)
$YbAl_4Na$	20.5(1)	1.62(9)	**$YbGa_4$**[5]	55.7(3)	5.88(2)
$Yb_2Al_8Na_2$	18.9(1)	1.6(1)	**Yb_2Ga_8**[10]	30.5(1)	2.43(6)
			$Yb_2Ga_8Na_2$[12]	37.1(1)	4.82(4)

[a]At room temperature, 2σ values between parentheses. Estimated experimental errors: τ_{obs}, ±2%; Q^L_{Ln} , ±10 %. [b]Under excitation at 355 nm. [c]Under excitation at 330 nm. [d]Under excitation at 350 nm.

Determination of the Triplet State

In the spirit of rationalizing the energy transfer, the lowest triplet state (T_1) of the organic ligands present in the MCs was analyzed. This electronic state is generally considered to play a major role in the sensitization of Ln^{III} emission.[22,23] It is therefore important to determine the energy of the T_1 state. Phosphorescence spectra of the corresponding Gd^{III} complexes are usually used for this purpose. The very high energy of the accepting energy level (32 000 cm^{-1})[24] of Gd^{III} prevents its population through the donating energy levels of most commonly used organic chromophores. In addition, the heavy-atom effect and the paramagnetic nature of Gd^{III} facilitate intersystem crossing[25], thus promoting the emission intensity from the triplet state. Phosphorescence spectra were acquired in time-resolved mode for **$GdAl_4Na$** and **$Gd_2Al_8Na_2$** in the solid state upon excitation at 330 nm (Fig. 7) in order to remove the short-live contribution of the fluorescence emission arising from the singlet state. These spectra revealed broad bands in the range of 420–750 nm with an additional resolved vibronic structure for the 0–0, 0–1, and 0–2 transitions (Table 3). The lowest energy transition (0–0) is a good approximation of the T_1 states of the MCs, and is located at 22 690 cm^{-1} for **$GdAl_4Na$** and at 21 360 cm^{-1} for **$Gd_2Al_8Na_2$**. These values are similar to the ones observed for the corresponding lanthanide-gallium MC analogues, i.e. 22 170 cm^{-1} for $(Hpy)Gd(ben)_4[12\text{-}MC_{Ga(III)N(shi)}\text{-}4]$[5], where Hpy^+ is pyridinium, 21 980 cm^{-1} for $(NH_4)_2\{Gd[12\text{-}MC_{Ga(III)N(shi)}\text{-}4]\}_2(iph)_4$[9], and 22 385 cm^{-1} for $\{GdNa[12\text{-}MC_{Ga(III)N(shi)}\text{-}4]\}_2(iph)_4$.[12]

Table 3. Energies of 0–0, 0–1 and 0–2 phonon transitions observed in the phosphorescence spectra of **$GdAl_4Na$** and **$Gd_2Al_8Na_2$** collected in the solid state at 77 K under ligand excitation.

Gd^{III} MC	E (cm^{-1})					
	0-0	0-1	0-2	$\Delta_{0\text{-}1}$	$\Delta_{1\text{-}2}$	Δ_{av}[a]
$GdAl_4Na$	22 690	21 285	19 730	1405	1555	1480(75)
$Gd_2Al_8Na_2$	21 360	20 390	19 650	970	740	855(115)

[a] Standard deviation values between parentheses.

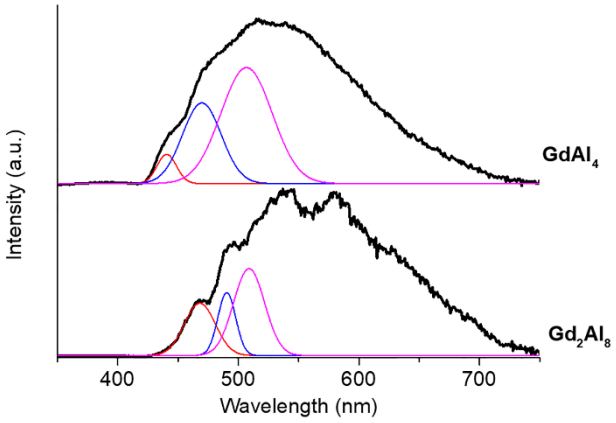

Figure 7. Corrected and normalized phosphorescence spectra of **$GdAl_4Na$** and **$Gd_2Al_8Na_2$** acquired in the solid state upon excitation at 330 nm and applying a 200 µs delay for the collection of the signal after the excitation flash at 77 K (black traces). 0–0 (red), 0–1 (blue) and 0–2 (magenta) phonon transitions were fitted with a Gaussian function.

Comparison to $(Hpy)Ln(ben)_4[12\text{-}MC_{Ga(III)N(shi)}\text{-}4]$ and $(NH_4)_2\{Ln[12\text{-}MC_{Ga(III)N(shi)}\text{-}4]\}_2(iph)_4$ Metallacrown Compounds

While not exact structural analogues, a series of gallium-lanthanide MCs has been reported by us. Gallium-lanthanide MC structures have been reported for both the discrete monomers and for the dimers. The structures are nearly isostructural to the aluminium-lanthanide MCs except for the nature of the countercation. In the **$LnAl_4Na$** and **$Ln_2Al_8Na_2$** structures, sodium ions are coordinated to the MCs to provide the charge balance. For the analogous gallium-lanthanide MCs, the uncoordinated countercation is either pyridinium for the $(Hpy)Ln(ben)_4[12\text{-}MC_{Ga(III)N(shi)}\text{-}4]$ monomers[5] (**$LnGa_4$**) or ammonium for the dimer $(NH_4)_2\{Ln[12\text{-}MC_{Ga(III)N(shi)}\text{-}4]\}_2(iph)_4$ molecules[10] (**Ln_2Ga_8**). One exception exists for the ytterbium-gallium dimer. In addition to the ammonium **Yb_2Ga_8** dimer, the structure and solid-state luminescence data of the corresponding sodium version, $\{YbNa[12\text{-}MC_{Ga(III)N(shi)}\text{-}4]\}_2(iph)_4$

(**$Yb_2Ga_8Na_2$**) has also been reported.[12] The comparison of the luminescence lifetimes and absolute quantum yields collected under ligand excitation (Table 2) reveals that for the erbium and ytterbium MCs, the gallium-based MCs tend to have longer lifetimes and higher quantum yield values than the analogous aluminum-based MCs. For the **$Er_2Al_8Na_2$** dimer, the quantum yield value is higher than the analogous **Er_2Ga_8** dimer; however, the **$Er_2Al_8Na_2$** dimer has a shorter lifetime. This implies that the non-radiative deactivation pathways are likely more significant for the **$Er_2Al_8Na_2$** dimer, but the sensitization efficiency of the erbium ions is possibly better. For the terbium MCs, there is not an absolute trend. **$TbAl_4Na$** and **$TbGa_4$** have similar luminescence lifetimes, while **$TbGa_4$** has a higher quantum yield. **Tb_2Ga_8** has a longer luminescence lifetime than **$Tb_2Al_8Na_2$,** though **$Tb_2Al_8Na_2$** has a significantly higher value for the quantum yield by around 40% (Table 2). At this time, it is difficult to establish a direct comparison of the solid-state luminescence data between the different types of terbium-based structures and to draw definitive conclusions. Part of the explanation lies in the amount of co-crystallized solvent molecules, in particular water, as the solvent is a strong source of non-radiative deactivation of the excited states of lanthanide cations. Moreover, the binding of the sodium ions to the **$Tb_2Al_8Na_2$** metallacrown may be a factor influencing the luminescent properties of this MC as the **Tb_2Ga_8** metallacrown contains two uncoordinated ammonium countercations. More detailed investigations need to be performed to elucidate the exact mechanism underlying the behavior of the terbium-based metallacrowns. Lastly, the **$LnAl_4Na$** and **$Ln_2Al_8Na_2$** compounds are unfortunately not readily soluble in common solvents, thus preventing any measurements in solution.

Conclusions

Two classes of 12-MC-4 compounds, $LnNa(ben)_4$[12-$MC_{Al(III)N(shi)}$-4] and {$LnNa$[12-$MC_{Al(III)N(shi)}$-4]}$_2(iph)_4$, where Ln = Gd^{III}, Tb^{III}, Er^{III}, and Yb^{III}, were investigated for their luminescent properties in the visible and in the near-infrared. In all cases, we observed that the emissions of the studied lanthanide ions were sensitized through the electronic structures of this novel family of metallacrowns. For the near-infrared emitting Er^{III} and Yb^{III} ions, both the monomer and dimer versions of each metal type have fairly similar luminescence lifetimes and quantum yield values. The terbium-based MCs displayed emission in the visible region with the dimer version having a quantum yield 1.8 times larger than the one of the discrete monomer. The quantum yield of the terbium dimer MC has a remarkable value of 43.9%, which is as of date the highest value measured for a terbium metallacrown in the solid state. These results demonstrate that light-weight *p*-block metals can indeed be incorporated into the MC framework and are suitable for the generation of luminescent lanthanide compounds with promising properties.

Author Contributions

S.V. Elisseva – Conceptualization, Funding Acquisition, Investigation, Data Curation, Formal Analysis, Writing – Original Draft

J.R. Travis, S. G. Nagy, A. M. Smihosky, C. M. Foley, and A. C. Kauffman – Investigation

C.M. Zaleski – Conceptualization, Funding Acquisition, Supervision, Writing – Review & Editing

S. Petoud - Conceptualization, Funding Acquisition, Supervision, Writing – Review & Editing

Conflicts of interest

There are no conflicts to declare.

Acknowledgements

CMZ would like to thank the following for financial support: the PASSHE Faculty Professional Development Council Grant Program, the Shippensburg University (SU) Faculty Professional Development Council Grant Program, the SU Student/Faculty Research Engagement Grant, the SU Miklausen-Likar Science Research Fund, the SU Summer Undergraduate Research Experience Program, and the SU and Shippensburg Foundation Undergraduate Research Program. The work in France was supported by La Ligue Contre le Cancer (comité du Loiret et d'Eure-et-Loir), the network ''Molécules marines, métabolisme et cancer'' from the Cancéropôle Grand Ouest, and la Région Centre Val de Loire. SP thanks the Institut National de la Santé et de la Recherche Médicale.

Notes and references

1 (a) G. Mezei, C. M. Zaleski, and V. L. Pecoraro, *Chem. Rev.* 2007, **107**, 4933-5003. (b) J. C. Lutter, C. M. Zaleski, and V. L. Pecoraro, In *Advances in Inorganic Chemistry*, eds. *R.* van Eldik and R. Puchta, Academic Press, Cambridge, MA, Vol. 71, 2018, 177-246. (c) T. N. Nguyen and V. L. Pecoraro, In *Comprehensive Supramolecular Chemistry II*, ed. J. L. Atwood, Elsevier, Oxford, UK, Vol. 5, 2017, 195-212.

2 (a) C. M. Zaleski, E. C. Depperman, J. W. Kampf, M. L. Kirk, and V. L. Pecoraro, *Angew. Chem. Int. Ed.* 2004, **43**, 3911-3914. (b) C. M. Zaleski, J. W. Kampf, T. Mallah, M. L. Kirk, and V. L. Pecoraro, *Inorg. Chem.* 2007, **46**, 1954-1956. (c) C. M. Zaleski, E. C. Depperman, J. W. Kampf, M. L. Kirk, and V. L. Pecoraro, *Inorg. Chem.* 2006, **45**, 10022-10024. (d) A. A. Athanasopoulou, L. M. Carrella, and E. Rentschler, *Dalton Trans.* 2019, **48**, 4779-4783. (e) W. Yang, H. Yang, S.-Y. Zeng, D.-C. Li, and J.-M. Dou, *Dalton Trans.* 2017, **46**, 13027-13034. (f) H. Yang, Y.-X. Meng, H.-Q. Tian, D.-C. Li, S.-Y. Zeng, Y. Song, and J.-M. Dou, *Dalton Trans.* 2020, **49**, 1955-1962. (g) G.-J. Zhou, T. Han, Y.-S. Ding, N. F. Chilton, and Y.-Z. Zheng, *Chem. Eur. J.* 2017, **23**, 15617-15622. (h) J. Wang, G. Lu, Y. Liu, S.-G. Wu, G.-Z. Huang, J.-L. Liu, and M.-L. Tong, *Cryst. Growth Des.* 2019, **19**, 1896-1902. (i) H. Yang, Z. Liu, Y. Meng, S. Zeng, Y. Li, and J. Dou, *J. Mol. Struct.* 2020, **1221**, 128822. (j) J. Wang, Z.-Y. Ruan, Q.-W. Li, Y.-C. Chen, G.-Z. Huang, J.-L. Liu, D. Reta, N. F. Chilton, Z.-X. Wang, and M.-L. Tong, *Dalton Trans.* 2019, **48**, 1686-1692. (k) J. Wang, Q.-W. Li, S.-G. Wu, Y.-C. Chen, R.-C. Wan, G.-Z. Huang, Y. Liu, J.-L. Liu, D. Reta, M. J. Giansiracusa, Z.-X. Wang, N. F. Chilton, and M.-L. Tong, *Angew. Chem. Int. Ed.* 2021, **60**, 5299-5306.

3 T. T. Boron, III, J. C. Lutter, C. I. Daly, C. Y. Chow, A. H. Davis, R. Nimthong-Roldán, M. Zeller, J. W. Kampf, C. M. Zaleski, and V. L. Pecoraro, *Inorg. Chem.* 2016, **55**, 10597 – 10607.

4 (a) M. R. Azar, T. T. Boron, III, J. C. Lutter, C. I. Daly, K. A. Zegalia, R. Nimthong, G. M. Ferrence, M. Zeller, J. W. Kampf, V. L. Pecoraro, and C. M. Zaleski, *Inorg. Chem.* 2014, **53**, 1729 – 1742. (b) J. R. Travis, M. Zeller, and C. M. Zaleski, *Acta Cryst.* 2015, **E71**, 1300 – 1306. (c) J. R. Travis, M. Zeller, and C. M. Zaleski, *Polyhedron* 2016, **114**, 29 – 36. (d) E. C. Manickas, M. Zeller, and C. M. Zaleski, *Acta Cryst.* 2020, **E76**, 1213 – 1221. (e) C. H. Michael, M. Zeller, and C. M. Zaleski, *J. Chem. Crystallogr.* 2021, **51**, 562-574.

5 C. Y. Chow, S. V. Eliseeva, E. R. Trivedi, T. N. Nguyen, J. W. Kampf, S. Petoud, and V. L. Pecoraro, *J. Am. Chem. Soc.* 2016, **138**, 5100-5109.

6 a) X. Wang, R. R. Valiev, T. Y Ohulchanskyy, H. Ågren, C, Yang, and G. Chen, *Chem. Soc. Rev.* 2017, **46**, 4150-4167. (b) Y. Ning, M. Zhu, and J.-L. Zhang, *Coord. Chem. Rev.* 2019, **399**, 213028. (c) U. Cho and J. K. Chen, *Cell Chem. Biol.* 2020, **27**, 921-936. (d) J.-C. G. Bünzli and S. V. Eliseeva, *Chem. Sci.* 2013, **4**, 1939-1949. (e) J.-C. G. Bünzli, A.-S. Chauvin, H. K. Kim, E. Deiters, and S. V. Eliseeva, *Coord. Chem. Rev.* 2010, **254**, 2623-2633.

7 (a) D.-F. Lu, Z.-F. Hong, J. Xie, X.-J. Kong, L.-S. Long, and L.-S. Zheng, *Inorg. Chem.* 2017, **56**, 12186-12192. (b) Y.-R. Zhao, H. Zheng, L.-Q. Chen, H.-J. Chen, X.-J. Kong, L.-S. Long, and L.-S. Zheng, *Inorg. Chem.* 2019, **58**, 10078-10083. (c) Y. Hasegawa and Y. Kitagawa, *J. Mater. Chem. C* 2019, **7**, 7494-7511. (d) X.-P. Shu, W. Luo, H.-Y. Wang, M.-Y. Fu, Q.-Y. Zhu, and J. Dai, *Inorg. Chem.* 2020, **59**, 10422-10429. (e) H. Li, X. Xu, Z. Tang, J. Zhao, L. Chen, and G.-Y. Yang, *Inorg. Chem.* 2021, **60**, 18065-18074. (f) D. A. Gálico and M. Murugesu, *ACS Appl. Mater. Interfaces* 2021, **13**, 47052-47060. (g) H.-P. Xiao, R.-T. Zhang, Z. Li, Y.-F. Xie, M. Wang, Y.-D. Ye, C. Sun, Y.-Q. Sun, X.-X. Li, and S.-T. Zheng, *Inorg. Chem.* 2021, **60**, 13715-13726.

8 E. Rajczak, V. L. Pecoraro, and B. Juskowiak, *Metallomics* 2017, **9**, 1735-1744.

9 S. V. Eliseeva, E. V. Salerno, B. A. Lopez Bermudez, S. Petoud, and V. L. Pecoraro, *J. Am. Chem. Soc.* 2020, **142**, 16173-16176.

10 T. N. Nguyen, C. Y. Chow, S. V. Eliseeva, E. R. Trivedi, J. W. Kampf, I. Martinić, S. Petoud, and V. L. Pecoraro, *Chem. Eur. J.* 2018, **24**, 1031-1035.

11 E. V. Salerno, J. Zeler, S. V. Eliseeva, M. A. Hernández-Rodríguez, A. N. Carneiro Neto, S. Petoud, V. L. Pecoraro, and L. D. Carlos, *Chem. Eur. J.* 2020, **26**, 13792-13796.

12 J. C. Lutter, S. V. Eliseeva, G. Collet, I. Martinić, J. W. Kampf, B. Schneider, A. Carichner, J. Sobilo, S. Lerondel, S. Petoud, and V. L. Pecoraro, *Chem. Eur. J.* 2020, **26**, 1274-1277.

13 C. M. Foley, M. A. Armanious, A. M. Smihosky, M. Zeller, and C. M. Zaleski, *J. Chem. Crystallogr.* 2021, **51**, 465-482.

14 (a) X.-J. Zhao, D.-C. Li, Q.-F. Zhang, D.-Q. Wang, and J.-M. Dou, *Inorg. Chem. Commun.* 2010, **13**, 346–349. (b) X.-J. Zhao, Q.-F. Zhang, D.-C. Li, J.-M. Dou, and D.-Q. Wang, *J. Organomet. Chem.* 2010, **695**, 2134–2141.

15 (a) J. Kübel, P. J. W. Elder, H. A. Jenkins, and I. Vargas-Baca, *Dalton Trans.* 2010**,** **39**, 11126–11128. (b) P. C. Ho, P. Szydlowski, J. Sinclair, P. J. W. Elder, J. Kübel, C. Gendy, L. M. Lee, H. Jenkins, J. F. Britten, D. R. Morim, and I. Vargas-Baca, *Nat. Commun.* 2016, **7**, 11299. (c) P. C. Ho, J. Rafique, J. Lee, L. M. Lee, H. A. Jenkins, J. F. Britten, A. L. Braga, and I. Vargas-Baca, *Dalton Trans.* 2017, **46**, 6570–6579. (d) P. C. Ho, R. Bui, A. Cevallos, S. Sequeira, J. F. Britten, and I. Vargas-Baca, *Dalton Trans.* 2019, **48**, 4879-4886. (e) J. Wang, P. C. Ho, J. F. Britten, V. Tomassetti, and I. Vargas-Baca, *New J. Chem.* 2019, **43**, 12601–12608.

16 R. D. Shannon, *Acta Cryst.* 1976, **A32**, 751-767.

17 J. R. Travis, A. M. Smihosky, A. C. Kauffman, S. E. Ramstrom, A. J. Lewis, S. G. Nagy, R. E. Rheam, M. Zeller, and C. M. Zaleski, *J. Chem. Crystallogr.* 2021, **51**, 372-393.

18 M. Llunell, D. Casanova, J. Cirera, P. Alemany, and S. Alvarez, SHAPE (version 2.1), Barcelona, Spain, 2013.

19 E. V. Salerno, S. V. Eliseeva, B. L. Schneider, J. W. Kampf, S. Petoud, and V. L. Pecoraro, *J. Phys. Chem. A* 2020, **124**, 10550-10564.

20 T. N. Nguyen, S. V. Eliseeva, C. Y. Chow, J. W. Kampf, S. Petoud, and V. L. Pecoraro, *Inorg. Chem. Front.* 2020, **7**, 1553-1563.

21 J. C. Lutter, S. V. Eliseeva, J. W. Kampf, S. Petound, and V. L. Pecoraro, *Chem. Eur. J.* 2018, **24**, 10773-10783.

22 S. I. Weissman, *J. Chem. Phys.* 1942, **10**, 214-217.

23 J.-C. G. Bünzli and S. V. Eliseeva, In *Comprehensive Inorganic Chemistry II*, ed. Yam, V. W. W., Elsevier, Amsterdam, Vol. 8, 2013, 339-398.

24 W. T. Carnall, P. R. Fields, and K. Rajnak, *J. Chem. Phys.* 1968, **49**, 4443-4446.

25 S. Tobita, M. Arakawa, and I. Tanaka, *J. Phys. Chem.* 1985, **89**, 5649-5654.